Available online at www.sciencedirect.com
ScienceDirect
Journal of Organometallic Chemistry 693 (2008) 1096–1108
Journal of Organometallic Chemistry
www.elsevier.com/locate/jorganchem

Synthesis, spectroscopic and electronic characterizations of two half sandwich ruthenium(II) complexes with 2-(2′-hydroxyphenyl)-benzoxazole and 4-picolinic acid ligands

J.G. Małecki [a,*], R. Kruszynski [b], M. Jaworska [c], P. Lodowski [c], Z. Mazurak [d]

[a] Department of Inorganic and Coordination Chemistry, Institute of Chemistry, University of Silesia, 9th Szkolna Street, 40-006 Katowice, Poland
[b] X-ray Crystallography Laboratory, Institute of General and Ecological Chemistry, Technical University of Łódź, 116 Żeromski Street, 90-924 Łódź, Poland
[c] Department of Theoretical Chemistry, Institute of Chemistry, University of Silesia, 9th Szkolna Street, 40-006 Katowice, Poland
[d] Polish Academy of Sciences, Centre of Polymer Chemistry, M. Sklodowskiej-Curie 34, Zabrze 41-819, Poland

Received 20 November 2007; received in revised form 20 December 2007; accepted 2 January 2008
Available online 8 January 2008

Abstract

The $[(C_6H_6)RuCl(HPB)]$ and $[(C_6H_6)RuCl_2(C_5H_4NCOOH)]$ complexes have been prepared and studied by IR, UV–Vis spectroscopy and X-ray crystallography. The complexes was prepared in reaction of $[(C_6H_6)RuCl_2]_2$ with 2-(2′-hydroxyphenyl)-benzoxazole or 4-picolinic acid in methanol. The electronic spectra of the obtained compounds have been calculated using the TDDFT method. The luminescence property of the half sandwich complex $[(C_6H_6)RuCl(HPB)]$ was studied by the DFT method and the mechanism was suggested.

Keywords: Ruthenium arene complexes; 2-(2′-Hydroxyphenyl)-benzoxazole; X-ray structure; Luminescence; DFT; TDFFT

1. Introduction

Ruthenium complexes containing nitrogen donor ligands have been shown to be effective catalysts for oxidations reactions [1–9], and the ruthenium compound with oxazoline molecules have been shown to tune the properties of a metal catalyst [10–15].

The phenolate oxygen of 2-(2′-hydroxyphenyl)-benzoxazole is capable of stabilizing higher oxidation states of the metal ion by sigma donation [16] which is very important in several catalytic process [17–20]. The use of bidentate ligands which incorporate nitrogen imine and phenolate oxygen donors seems appropriate for synthesizing ruthenium complexes essential from the catalytic point of view.

On the other hand, the 2-(2′-hydroxyphenyl)-benzoxazole (HBO) ligand is a typical compound exhibiting excited state intramolecular proton transfer (ESIPIT) [21]. Excited-state proton transfer plays an important role in a large variety of photoinduced chemical and biological processes. A photoreaction in DNA, in which the equilibrium between keto-amine and enol-imine forms of the base pairs is established by double proton transfer [22], is very interesting. The HBO plays an important role in the fluorescent dyes that exhibit excited state intramolecular proton transfer reactions. These dyes have attracted great interest for several decades because such compounds show good photophysical properties such as intense fluorescence, large Stokes shifts and significant photostability [23–25].

The 2-(2′-hydroxyphenyl)-benzoxazole (HBO) ligand is in focus of the theoretical scientists due to its many applications such as laser dyes and UV stabilizers [26].

The second type of ligand – picolinic acids – plays a very important role in biochemistry [27] and organometalic chemistry [28].

* Corresponding author. Tel./fax: +48 32 255911.
E-mail addresses: gmalecki@us.edu.pl (J.G. Małecki), rafal.kruszynski@p.lodz.pl (R. Kruszynski), mj@tc3.ich.us.edu.pl (M. Jaworska), mazurak@cchp-pan.zabrze.pl (Z. Mazurak).

0022-328X/$ - see front matter © 2008 Elsevier B.V. All rights reserved.
doi:10.1016/j.jorganchem.2008.01.001

Table 1
Crystal data and structure refinement details of $[(C_6H_6)RuCl(HPB)]$ (**1**) and $[(C_6H_6)RuCl_2(C_5H_4NCOOH)] \cdot CH_3OH$ (**2**)

	1	**2**
Empirical formula	$C_{19}H_{14}ClNO_2Ru$	$C_{13}H_{15}Cl_2NO_3Ru$
Formula weight	424.83	405.23
Temperature (K)	291.0(3)	291.0(3)
Crystal system	Orthorhombic	Monoclinic
Space group	$Pna2_1$	$P2_1/n$
Unit cell dimensions		
a (Å)	8.5597(9)	7.4468(4)
b (Å)	12.8697(11)	30.1834(17)
c (Å)	14.3632(13)	7.5017(4)
β		115.992(4)
Volume (Å^3)	1582.3(3)	1515.61(14)
Z	4	4
D_{calc} (Mg/m^3)	1.783	1.776
Absorption coefficient (mm^{-1})	1.170	1.391
$F(000)$	848	808
Crystal dimensions (mm)	$0.441 \times 0.420 \times 0.411$	$0.063 \times 0.009 \times 0.007$
θ Range for data collection (°)	3.19–25.00	2.00–20.00
Index ranges	$-9 \leqslant h \leqslant 10$, $-15 \leqslant k \leqslant 15$, $-17 \leqslant l \leqslant 17$	$-8 \leqslant h \leqslant 8$, $-35 \leqslant k \leqslant 34$, $-8 \leqslant l \leqslant 8$
Reflections collected	15483	14612
Independent reflections [$R_{(int)}$]	2771 [0.0504]	2669 [0.0631]
Data/restraints/parameters	2771/1/217	2669/0/184
Goodness-of-fit on F^2	1.075	1.007
Final R indices [$I > 2\sigma(I)$]	$R_1 = 0.0500$, $wR_2 = 0.1236$	$R_1 = 0.0625$, $wR_2 = 0.1039$,
R indices (all data)	$R_1 = 0.0503$, $wR_2 = 0.1239$	$R_1 = 0.1103$, $wR_2 = 0.1168$
Largest difference in peak and hole (e Å^{-3})	1.228 and −0.816	0.830 and −0.521

In this paper, we report the synthesis, spectroscopic (absorption and emission) and electronic properties of the half sandwich ruthenium complexes containing the HBO and 4-picolinic acid ligands.

2. Experimental

All reagents were commercially available and were used without further purification.

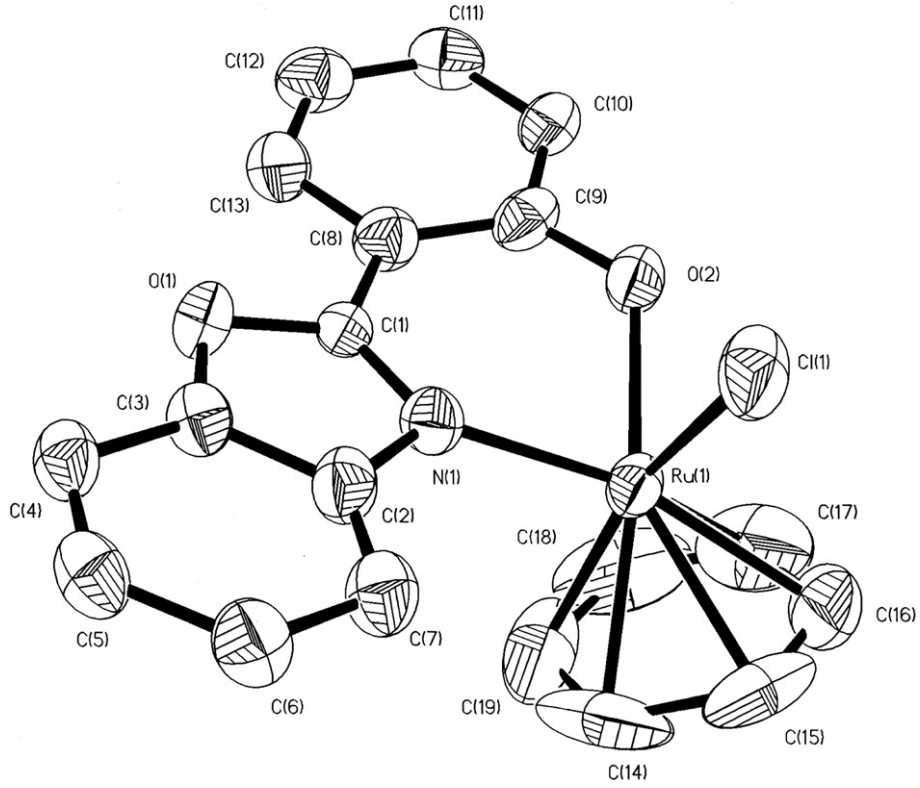

Fig. 1. ORTEP drawing of $[(C_6H_6)RuCl(HBO)]$ with 50% probability thermal ellipsoids.

2.1. Synthesis of $[(C_6H_6)RuCl(HBO)]$ (**1**) and $[(C_6H_6)RuCl_2(C_5H_4NCOOH)] \cdot CH_3OH$ (**2**)

Both complexes are synthesized in the reaction between $[(C_6H_6)RuCl_2]_2$ (0.25 g; 5×10^{-4} mol) and 2-(2′-hydroxy-

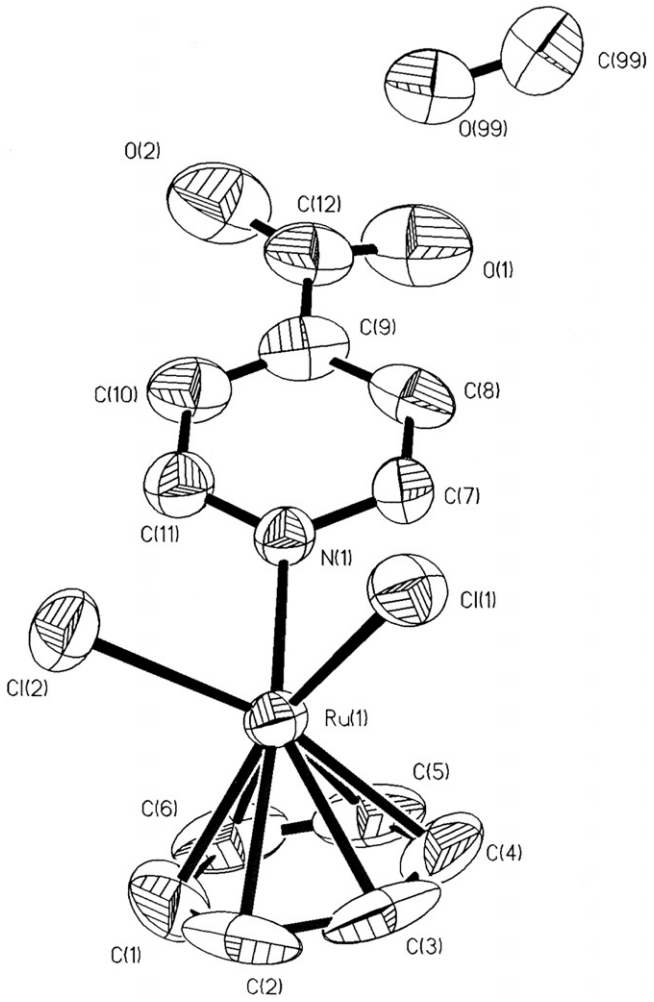

Fig. 2. ORTEP drawing of $[(C_6H_6)RuCl_2(C_5H_4NCOOH)] \cdot CH_3OH$ with 50% probability thermal ellipsoids.

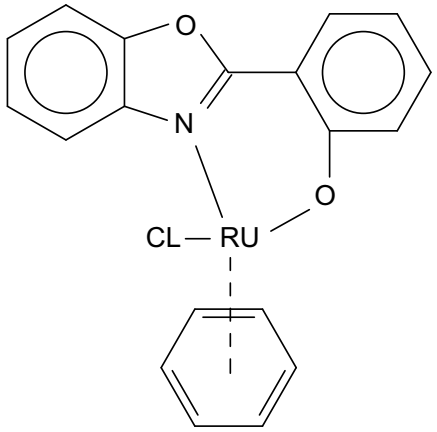

Fig. 3. Structural drawing of $[(C_6H_6)RuCl(HBO)]$.

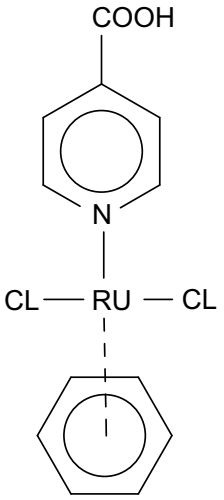

Fig. 4. Structural drawing of $[(C_6H_6)RuCl_2(C_5H_4NCOOH)]$.

Table 2
Selected bond lengths (Å) and angles (°) for $[(C_6H_6)RuCl(HBP)]$ (**1**) and $[(C_6H_6)RuCl_2(C_5H_4NCOOH)]$ (**2**)

1		**2**	
Bond lengths (Å)			
Ru(1)–N(1)	2.080(6)	Ru(1)–N(1)	2.149(6)
Ru(1)–O(2)	2.099(6)	Ru(1)–Cl(1)	2.4148(17)
Ru(1)–C(19)	2.136(11)	Ru(1)–Cl(2)	2.407(2)
Ru(1)–C(14)	2.157(8)	Ru(1)–C(1)	2.155(8)
Ru(1)–C(17)	2.161(11)	Ru(1)–C(2)	2.178(8)
Ru(1)–C(18)	2.162(11)	Ru(1)–C(3)	2.169(8)
Ru(1)–C(15)	2.182(9)	Ru(1)–C(4)	2.150(9)
Ru(1)–C(16)	2.202(8)	Ru(1)–C(5)	2.150(9)
Ru(1)–Cl(1)	2.414(2)	Ru(1)–C(6)	2.161(8)
Angles (°)			
N(1)–Ru(1)–O(2)	83.4(2)	N(1)–Ru(1)–Cl(1)	85.42(15)
N(1)–Ru(1)–C(18)	114.7(6)	N(1)–Ru(1)–Cl(2)	87.45(17)
N(1)–Ru(1)–C(14)	98.6(4)	Cl(2)–Ru(1)–Cl(1)	86.52(7)
N(1)–Ru(1)–C(16)	164.6(4)	N(1)–Ru(1)–C(2)	162.8(4)
N(1)–Ru(1)–Cl(1)	86.56(18)	N(1)–Ru(1)–C(4)	110.8(4)
O(2)–Ru(1)–Cl(1)	85.44(19)	N(1)–Ru(1)–C(6)	94.8(3)
O(2)–Ru(1)–C(14)	159.7(7)	C(2)–Ru(1)–Cl(2)	96.1(3)
O(2)–Ru(1)–C(16)	111.9(4)	C(4)–Ru(1)–Cl(2)	161.8(4)
O(2)–Ru(1)–C(18)	91.8(4)	C(6)–Ru(1)–Cl(2)	111.4(4)
C(14)–Ru(1)–Cl(1)	114.8(7)	C(2)–Ru(1)–Cl(1)	111.6(4)
C(16)–Ru(1)–Cl(1)	96.0(4)	C(4)–Ru(1)–Cl(1)	95.1(3)
C(18)–Ru(1)–Cl(1)	158.1(7)	C(6)–Ru(1)–Cl(1)	162.1(4)
C(14)–Ru(1)–C(18)	68.9(6)	C(2)–Ru(1)–C(4)	68.2(4)
C(14)–Ru(1)–C(16)	66.5(4)	C(2)–Ru(1)–C(6)	68.1(4)
C(18)–Ru(1)–C(16)	65.0(6)	C(4)–Ru(1)–C(6)	66.4(4)

Table 3
Hydrogen Bonds in $[(C_6H_6)RuCl_2(C_5H_4NCOOH)]$ (**2**)

D–H···A	*d*(D–H)	*d*(H···A)	*d*(D···A)	∠(DHA)
O(1)—H(1A)O(99)#1	0.82	1.87	2.628(11)	153.0
O(99)—H(99)Cl(2)	0.82	2.79	3.442(11)	136.0
C(2)—H(2)Cl(1)#2	0.93	2.79	3.695(14)	164.0
C(5)—H(5)O(99)#3	0.93	2.57	3.418(16)	152.0
C(11)—H(11)Cl(2)	0.93	2.75	3.259(12)	115.0

Distances are in (Å) and angles are in (°).
Symmetry operators used to generate equivalent atoms: #1 $1/2 + x$, $1/2 - y$, $-1/2 + z$; #2 $-x$, $-y$, $1 - z$; #3 x, y, $-1 + z$.

phenyl)-benzoxazole (0.21 g; 1×10^{-3} mol) or 4-picolinic acid (0.13 g; 1×10^{-3} mol) in refluxed methanol (150 cm^3) until the ruthenium dimer dissolved. Than the solution is cooled and filtered. The crystals suitable for X-ray crystal analysis are obtained by slow evaporation of the reaction mixture **1** and the complex **2** was recrystallized from the mixture methanol:ethanol:1-propanol (85:10:5 v/v).

$[(C_6H_6)RuCl(HBO)]$ – Yield 68%. Colour: red. IR (KBr): 3072, 3031 (ν_{CH}), 1632 (ν_{CN}), 1545, 1489 (ν_{ring}), 1063, 1000, 799 (δ_{CH}). UV–Vis (CH_3CN, λ nm): 372.6 (2.88), 292.3 (3.01), 248.3 (3.26), 230.90 (3.39), 207.6 (4.03). Anal. Calc. for $C_{18}H_{14}ClNO_2Ru$: C, 52.37; H, 3.42; Cl, 8.59; N, 3.39; O, 7.75; Ru, 24.48. Found: C, 52.3; H, 3.29; N, 3.35%.

$[(C_6H_6)RuCl_2(C_5H_4COOH)]$ – Yield 74%. Colour: orange. IR (KBr): 3055 (ν_{CH}), 2415 (ν_{OH}), 1725 ($\nu_{C=O}$), 1616 (ν_{CN}), 1559 (as ν_{COO}), 1412 (s ν_{COOH}), 1233 (δ_{CH}). UV–Vis (CH_3CN, λ nm): 420.4 (2.78), 295.8 (3.06), 272.2 (3.21), 220.10 (3.31), 202.6 (4.01). Anal. Calc. for $C_{19}H_{21}Cl_2NO_3Ru$: C, 47.21; H, 4.38; Cl, 14.67; N, 2.90; O, 9.93; Ru, 20.91. Found: C, 47.32; H, 4.31; N, 2.81%.

2.2. Physical measurements

Infrared spectra were recorded on a Nicolet Magna 560 spectrophotometer in the spectral range 4000–400 cm^{-1} with the sample in the form of KBr pellet. Electronic spectra were measured on a Lab Alliance UV–Vis 8500 spectrophotometer in the range of 600–180 nm in deoxygenated acetonitrile solution. Elemental analyses (C, H, N) were performed on a Perkin–Elmer CHN-2400 analyzer. The ^1H NMR spectrum was obtained at room temperature in $CDCl_3$ using an INOVA 300 spectrometer. Luminescence measurements were made on a Jobin-Yvon (SPEX) FLUOROLOG-3.12 spectrofluorometer at room temperature.

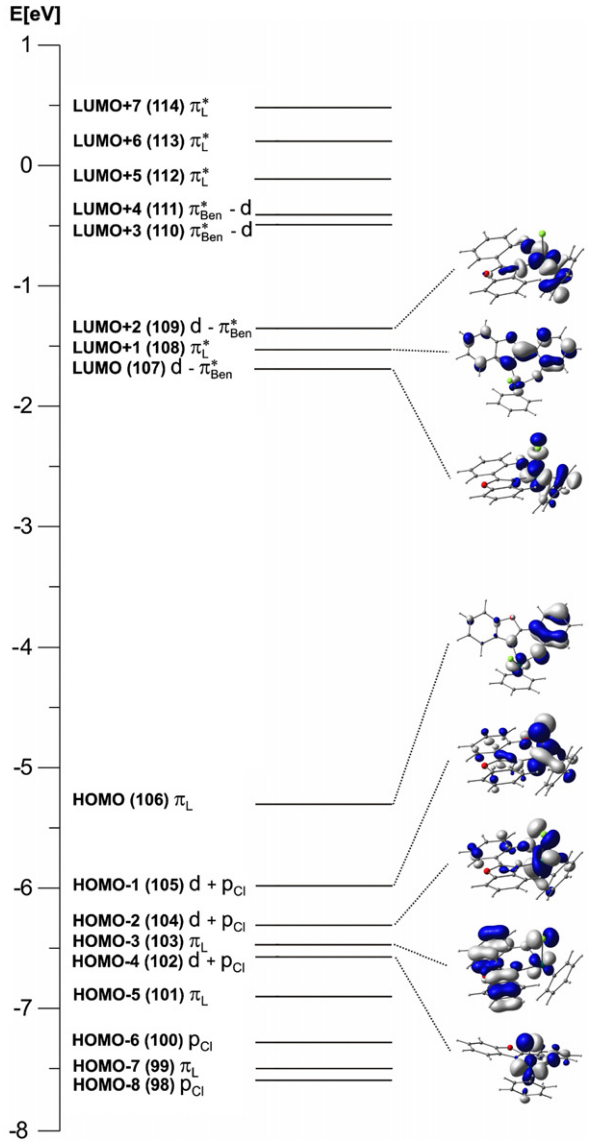

Fig. 6. Molecular orbital diagram for $[(C_6H_6)RuCl(HBO)]$.

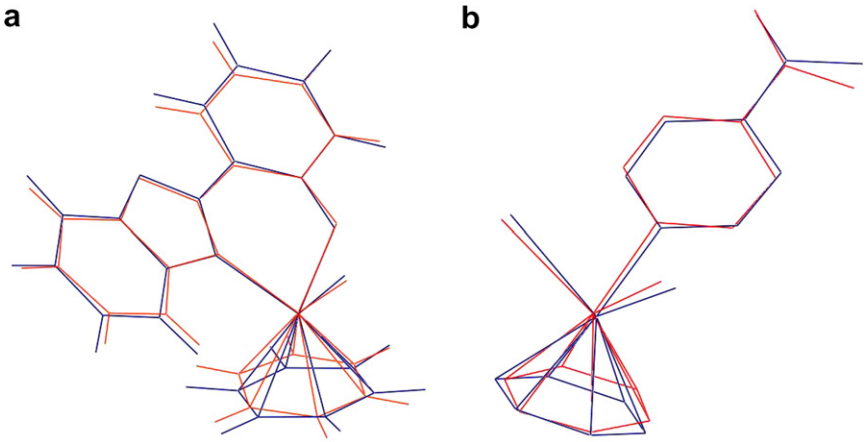

Fig. 5. The relative orientations of the experimental (blue) and optimized (red) molecules of $[(C_6H_6)RuCl(HBO)]$ (a) and $[(C_6H_6)RuCl_2(C_5H_4NCOOH)]$ (b) complexes. (For interpretation of the references to colour in this figure legend, the reader is referred to the Web version of this article.)

2.3. DFT calculations

The calculations were carried out using GAUSSIAN03 [27] and TURBOMOLE programs. The DFT/B3LYP [29,30] method was used for the geometry optimization and electronic structure determination, and electronic spectra were calculated by TDDFT [31] method. The calculations were performed using the DZVP basis set [32] with f functions with exponents 1.94722036 and 0.748930908 on ruthenium atom, and polarization functions for all other atoms: 6-31g(2d,p) – chlorine, 6-31g** – carbon, nitrogen and 6-31g(d,p) – hydrogen. The PCM solvent model was used in the Gaussian calculations and the COSMO solvent model – in the TURBOMOLE calculations, with acetonitrile as the solvent.

2.4. Crystal structures determination and refinement

A red prism crystal of $[(C_6H_6)RuCl(HBO)]$ (**1**) and an orange needle of $[(C_6H_6)RuCl_2(C_5H_4NCOOH)] \cdot CH_3OH$ (**2**) were mounted in turn on a KM-4-CCD automatic diffrac-

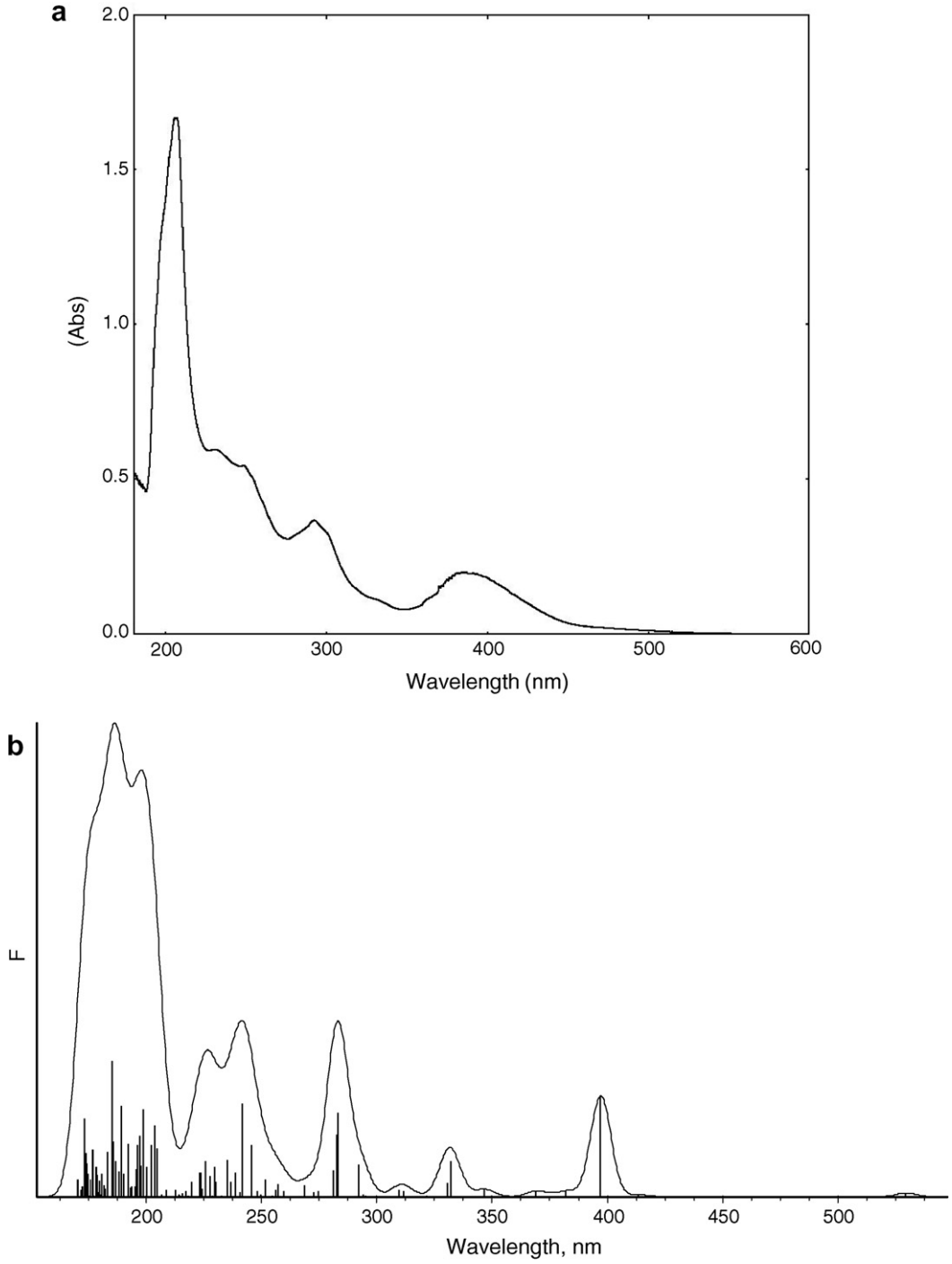

Fig. 7. The UV–Vis spectra of $[(C_6H_6)RuCl(HBO)]$ (a) experimental; (b) calculated.

tometer equipped with a CCD detector, and used for data collection. X-ray intensity data were collected with graphite-monochromated Mo Kα radiation ($\lambda = 0.71073$ Å) at temperature 291.0(3) K, with ω scan mode. The 33 s exposure times were used and Ewald sphere reflections were collected up to $2\theta = 50$. The unit cell parameters were determined from least-squares refinement of the setting angles of 6625 (**1**) and 13956 (**2**) strongest reflections. Details concerning crystal data and refinement are given in Table 1. Examination of 18 and 23 reflections on two reference frames monitored after each 20 frames measured showed 0.03% and 19.73% loss of the intensity respectively for **1** and **2**. During the data reduction, the above decay correction coefficient was taken into account. Lorentz, polarization, and numerical absorption [33] corrections were applied. The structures were solved by Patterson method. All the non-hydrogen atoms were refined anisotropically using full-matrix, least-squares technique on F^2. All the hydrogen atoms were found from difference Fourier synthesis after four cycles of anisotropic refinement, and refined as "riding" on the adjacent atom with individual isotropic temperature factor equal 1.2 times the value of equivalent temperature factor of the parent atom, with geometry idealization after each cycle. SHELXS97 [30], SHELXL97 [34] and SHELXTL [35] programs were used for all the calculations. Atomic scattering factors were those incorporated in the computer programs.

Table 4
The calculated singlet states for $[(C_6H_6)RuCl(HBP)]$ (**1**)

	E (eV)	λ (nm)	f	Weight	Character	Expt. λ (E)
S_1	2.27	545.2	0.0084	65	$106(\pi_L) \rightarrow 107(d)$	
S_2	2.58	480.7	0.0007	32	$105(d) \rightarrow 107(d)$	
				31	$106(\pi_L) \rightarrow 109(d)$	
S_3	2.75	451.3	0.0001	33	$105(d) \rightarrow 107(d)$	
				28	$106(\pi_L) \rightarrow 109(d)$	
S_4	2.94	421.6	0.0029	22	$104(d) \rightarrow 107(d)$	
				39	$105(d) \rightarrow 109(d)$	
S_5	3.16	392.1	0.1466	74	$106(\pi_L) \rightarrow 108(\pi_L^*)$	372 (3.33)
S_6	3.18	390.3	0.0197	30	$104(d) \rightarrow 107(d)$	
				15	$106(\pi_L) \rightarrow 107(d)$	
				10	$106(\pi_L) \rightarrow 109(d)$	
S_7	3.34	371.1	0.0143	21	$102(d) \rightarrow 109(d)$	
				21	$104(d) \rightarrow 109(d)$	
S_8	3.52	352.1	0.0293	48	$102(d) \rightarrow 107(d)$	
				12	$105(d) \rightarrow 109(d)$	
S_9	3.76	330.2	0.0064	26	$102(d) \rightarrow 109(d)$	
				20	$104(d) \rightarrow 109(d)$	
				13	$106(\pi_L) \rightarrow 109(d)$	
S_{10}	3.80	326.5	0.0623	75	$105(d) \rightarrow 108(\pi_L^*)$	
S_{16}	4.30	288.3	0.0566	59	$102(d) \rightarrow 108(\pi_L^*)$	
				19	$105(d) \rightarrow 110(\pi_{Ben}^*)$	
S_{17}	4.34	285.8	0.1025	39	$103(\pi_L) \rightarrow 108(\pi_L^*)$	292 (4.25)
				34	$103(\pi_L) \rightarrow 109(d)$	
S_{18}	4.41	281.1	0.1363	29	$103(\pi_L) \rightarrow 108(\pi_L^*)$	
				31	$103(\pi_L) \rightarrow 109(d)$	
S_{19}	4.46	278.2	0.0460	13	$100(p_{Cl}) \rightarrow 107(d)$	
				14	$104(d) \rightarrow 110(\pi_{Ben}^*)$	
				36	$105(d) \rightarrow 111(\pi_{Ben}^*)$	
S_{28}	4.96	249.8	0.0266	16	$102(d) \rightarrow 110(\pi_{Ben}^*)$	
				46	$106(\pi_L) \rightarrow 113(\pi_L^*)$	
S_{29}	4.97	249.5	0.0253	24	$102(d) \rightarrow 110(\pi_{Ben}^*)$	
				19	$104(d) \rightarrow 110(\pi_{Ben}^*)$	
				16	$106(\pi_L) \rightarrow 113(\pi_L^*)$	
S_{30}	5.00	247.8	0.0305	52	$97(d) \rightarrow 107(d)$	
S_{32}	5.03	246.4	0.1176	21	$100(p_{Cl}) \rightarrow 108(\pi_L^*)$	248 (5.00)
				38	$100(p_{Cl}) \rightarrow 109(d)$	
S_{36}	5.24	236.4	0.1313	13	$99(\pi_L) \rightarrow 108(\pi_L^*)$	230 (5.39)
				33	$106(\pi_L) \rightarrow 114(\pi_L^*)$	
S_{37}	5.28	235.0	0.0312	13	$104(d) \rightarrow 110(\pi_{Ben}^*)$	
				31	$105(d) \rightarrow 112(\pi_L^*)$	
S_{38}	5.37	230.9	0.0049	68	$103(\pi_L) \rightarrow 110(\pi_{Ben}^*)$	
S_{39}	5.39	229.9	0.0646	31	$98(p_{Cl}) \rightarrow 108(\pi_L^*)$	
				12	$98(p_{Cl}) \rightarrow 109(d)$	
				24	$99(\pi_L) \rightarrow 108(\pi_L^*)$	
S_{40}	5.42	228.9	0.0566	37	$98(p_{Cl}) \rightarrow 108(\pi_L^*)$	
				11	$99(\pi_L) \rightarrow 108(\pi_L^*)$	

3. Results and discussion

The reactions of the ruthenium(II) benzene complex $[(C_6H_6)RuCl_2]_2$ with 2-(2′-hydroxyphenyl)-benzoxazole and 4-pyridine carboxylic acid have been performed. Refluxing the $[(C_6H_6)RuCl_2]_2$ complex with a small excess of the ligands in methanol leads to the half-sandwich complexes: $[(C_6H_6)RuCl(HBO)]$, where HBO = 2-(2′-hydroxyphenyl)-benzoxazole, and $[(C_6H_6)RuCl_2(C_5H_4NCOOH)]$ with good yield. The elemental analysis of the complexes is in good agreement with their formulas. Infrared spectra of the complexes exhibit characteristic bands due to ligand rings vibrations. The $\nu_{C=N}$ band in the complexes appeared around 1632 (**1**) and 1616 cm^{-1} (**2**). Infrared spectrum of the complex **2** exhibits the characteristic bands of the COO stretching mode: asymmetric at 1559 cm^{-1} and symmetric at 1412 cm^{-1}.

3.1. Crystal structures

Both studied complexes adopt distorted piano-stool type of geometry. The $[(C_6H_6)RuCl(HBO)]$ (**1**) complex crystallizes in the orthorhombic space group $Pna2_1$ and the $[(C_6H_6)RuCl_2(C_5H_4COOH)]$ (**2**) crystallizes in the $P2_1/n$

Table 5
The lowest triplet states for $[(C_6H_6)RuCl(HBP)]$ (**1**)

	E (eV)	λ (nm)	Weight	Coefficient	Character
T_1	1.86	666.9	31	0.5589	$106(\pi_L) \rightarrow 107(d)$
T_2	2.12	584.0	29	0.5347	$105(d) \rightarrow 107(d)$
T_3	2.22	559.3	15	−0.3928	$105(d) \rightarrow 107(d)$
			18	0.4277	$106(\pi_L) \rightarrow 109(d)$
T_4	2.39	517.9	15	−0.3858	$102(d) \rightarrow 107(d)$
			22	0.4735	$104(d) \rightarrow 107(d)$
T_5	2.46	504.6	28	0.5319	$105(d) \rightarrow 109(d)$
T_6	2.55	485.8	46	0.6796	$106(\pi_L) \rightarrow 108(\pi_L^*)$
T_7	2.65	468.3	12	−0.3421	$102(d) \rightarrow 109(d)$
			27	0.5186	$104(d) \rightarrow 109(d)$
T_8	3.12	397.8	11	0.3339	$103(\pi_L) \rightarrow 108(\pi_L^*)$
			15	0.3923	$105(d) \rightarrow 108(\pi_L^*)$
T_9	3.21	385.9	15	0.3923	$102(d) \rightarrow 107(d)$
			14	−0.3706	$106(\pi_L) \rightarrow 107(d)$
T_{10}	3.50	354.1	14	−0.3707	$102(d) \rightarrow 109(d)$
			18	0.4210	$106(\pi_L) \rightarrow 109(d)$

monoclinic space group. The molecular structures of the compounds are shown in Figs. 1 and 2 (structural drawings are presented in Figs. 3 and 4). The selected bond lengths and angles are listed in Table 2.

In both complexes the ruthenium atom is π-bonded to the benzene ring with a distance between benzene centroid and ruthenium atom equal to 1.671 Å and 1.661 Å, respectively, in complexes **1** and **2**; this is consistent with the values reported for the other Ru(II) η^6-arene complexes [36–38]. In both cases, the benzene molecule shows typical distortion observed in this type of compounds (twisting about axis perpendicular to the benzene ring plane and going through ring centroid) [39], what manifests in relatively large benzene carbon displacement parameters. The benzooxazole moiety of **1** is slightly distorted from planarity (maximum deviation of −0.032(5) Å exists for atom N(1) and create an angle of 15.3(3)° with oxyphenyl group). The carboxylate group and pyridyl moiety of **2** are inclined at 12.6(9)°, and Ru(1) atom deviates 0.33(1) from the aromatic ring lest squares plane. The

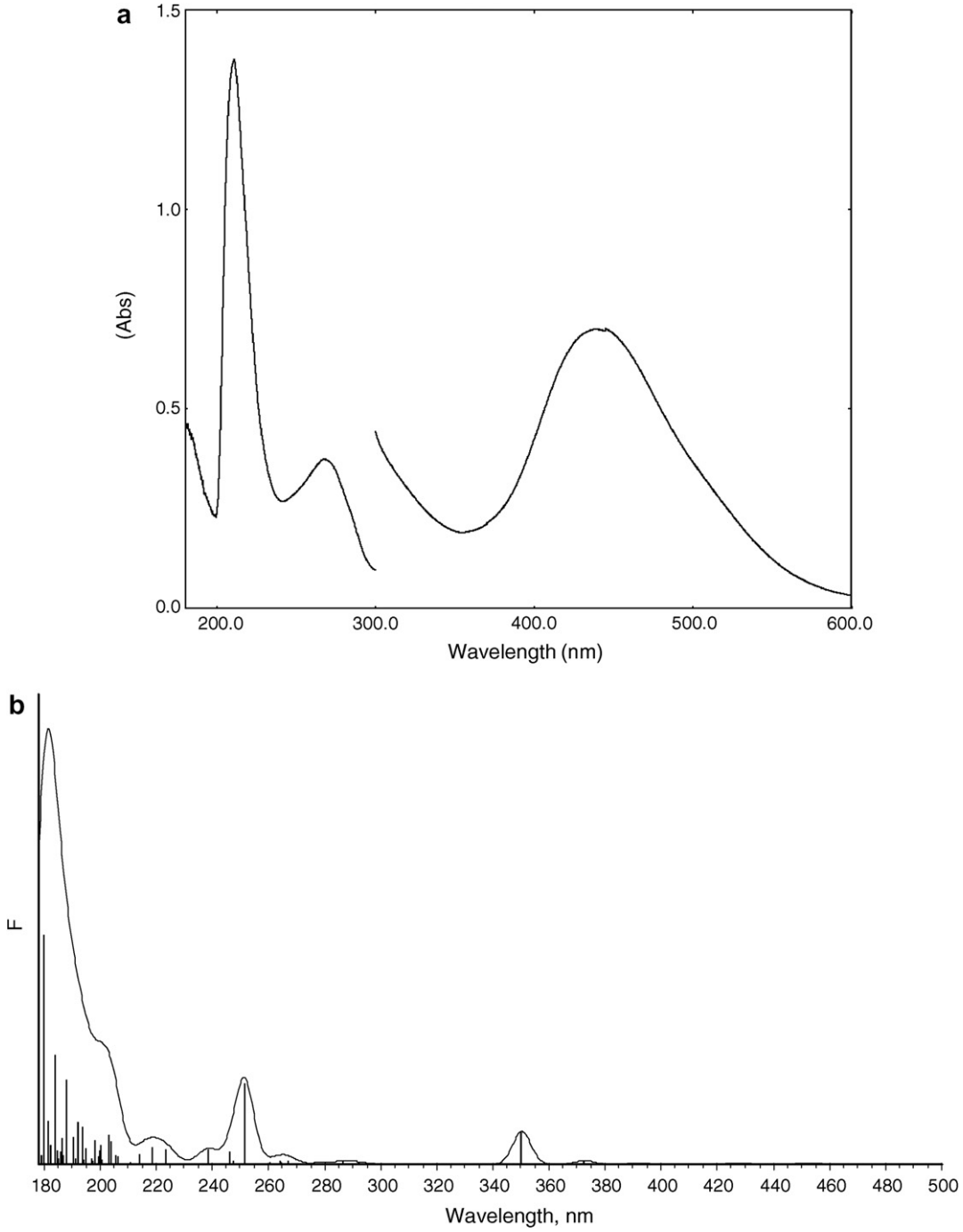

Fig. 8. The UV–Vis spectra of $[(C_6H_6)RuCl_2(C_5H_4NCOOH)]$ (a) experimental; (b) calculated.

bond lengths and angles in the studied complexes are comparable to those reported to analogues compounds [40].

In the structure of complex **1**, one short intramolecular interaction exists, which can be considered as a weak C(13)–H(13) ⋯ O(1) hydrogen bond [41–44] (D ⋯ A distance 2.819(10) Å, D–H ⋯ A angle 100.0°). In the complex **2**, multiple hydrogen bonds are observed (Table 3). In compound **2**, the parallel by symmetry benzene rings are connected via π•π stacking intersections (second ring obtained by $-x$, $-y$, $-z$ symmetry transformation, ring centroid distance is 3.472(9) Å, the angle between linking rings centroids vector and normal to one of planes is 14.3(6)°, perpendicular distance of one ring centroid to the second ring is 3.364(8) Å).

3.2. Geometry and electronic structure

The geometry of the studied compound **1** was optimized in a singlet state by the DFT method with the B3LYP functional with the solvent models both PCM and COSMO. The differences in obtained geometry parameters are rather small. The geometry of the complex **2** was optimized in PCM model.

The optimized and experimental structures of the complexes are presented in the Fig. 5. One may see in the figure that most of differences are visible in the benzene ring. The largest differences were found for the ruthenium–benzene carbons distances. The calculated Ru–benzene centroid distances are 1.733 Å for **1** and 1.725 Å for **2**. The maximum differences in the bond distances are visible between Ru(1)–C(14) and Ru(1)–C(19) 0.103 and 0.095 Å, respectively, for complex **1** and Ru(1)–C(4) and Ru(1)–C(6) 0.101 and 0.097 for **2**. In the case of the optimized angles, the maximum differences from the experimental value occur in the O(2)–Ru(1)–C(16) and C(14)–Ru(1)–Cl(1)–4.63 and 4.51° for compound **1** and Cl(2)–Ru(1)–Cl(1) and N(1)–Ru(1)–C(6)–3.61 and 4.05° for compound **2**.

The formal charge of the ruthenium atom is +2 in these complexes. The calculated charge on the ruthenium atom, obtained from natural population analysis, is close to 0.877 and 0.741 for complexes **1** and **2**, respectively. The population of the d_{xy}, d_{xz}, d_{yz}, $d_{x^2-y^2}$ and $d_z{}^2$ orbitals of the central atom in **1** is as follows: 1.022, 1.443, 1.845, 1.557 and 0.980, respectively. In the complex **2** the values are as follows: 1.579 (d_{xy}), 1.835 (d_{xz}), 1.003 (d_{yz}), 1.274 ($d_{x^2-y^2}$), 1.270 ($d_z{}^2$). This is a result of charge donation from ligands to metal center. The conclusion confirms the second-order perturbation analysis from NBO.

Each natural bond orbital (NBO) σ_{AB} can be written in terms of two directed valence hybrids (HHOs) h_A *i* h_B on atoms A and B:

$$\sigma_{AB} = c_A h_A + c_B h_B$$

where c_A *i* c_B are polarization coefficients. Each valence bonding NBO must in turn be paired with a corresponding valence antibonding NBO:

$$\sigma^*_{AB} = c_B h_A - c_A h_B$$

to complete the span of the valence space. The Lewis-type (donor) NBOs are thereby complemented by the non-Lewis-type (acceptor) NBOs that are formally empty in an idealized Lewis picture. The interactions between 'filled' Lewis-type NBOs and 'empty' non-Lewis NBOs lead to loss of occupancy from the localized NBOs of the idealized Lewis structure into the empty non-Lewis orbitals, and they are referred to as 'delocalization' corrections to the zeroth-order natural Lewis structure. The stabilization energy ΔE_{ij} (kcal/mol) associated with delocalization is estimated by the second-order perturbative as

$$\Delta E_{ij} = q_i(F(i,j)^2)/(\varepsilon_j - \varepsilon_i)$$

where q_i is the donor orbital occupancy, ε_i, ε_j are diagonal elements (orbital energies) and $F(i,j)$ is the off-diagonal NBO Fock or Kohn-Sham matrix element.

The stabilization energy calculated in this analysis has shown that the lone pairs localized on the chlorine ligand and nitrogen, oxygen atoms of benzoxazole ligand donate the charge to ruthenium d orbital, and the stabilization energy (ΔE_{ij}) is 156.38, 67.61, 58.32 kcal/mol, respectively. The donor–acceptor interactions between π bond linking C(15) and C(16) atoms in the benzene ring and ruthenium d orbital have the energy close to 60.63 kcal/mol. For the complex with 4-picolinic acid as the ligand, the donation of charge to ruthenium is mainly visible between chloride ion and lone pair of picolinic nitrogen; the stabilization energy is close to 91.90 and 75.18 kcal/mol, respectively. The stabilization energy of the charge donation from benzene ring to antibonding d orbitals is in the range of 43.02–48.57 kcal/mol.

The HOMO–LUMO gaps are 3.58 and 3.77 eV for complexes **1** and **2**, respectively.

In Fig. 6, the molecular orbital diagram for complex **1** is presented. The HOMO orbital is a ligand π orbital local-

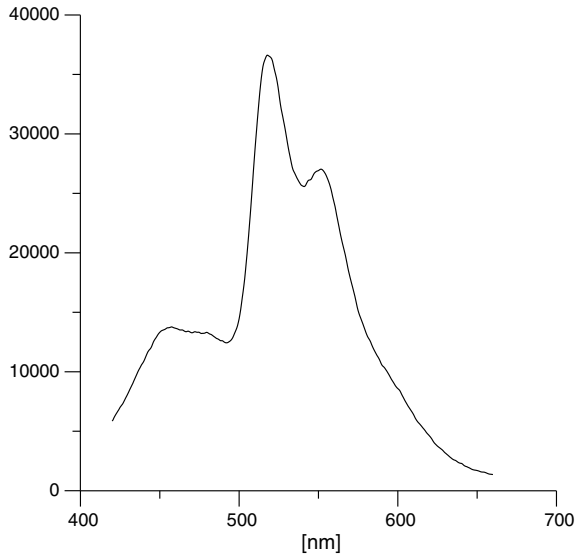

Fig. 9. The emission spectrum of [RuCl(CO)$(PPh_3)_2(C_9H_6NO)$].

ized on the phenolate ring. HOMO−1 and HOMO−2 are d orbitals with admixture of chlorine orbitals. LUMO and LUMO+2 are d orbitals in antibonding combination with benzene π orbitals. LUMO+1 is a ligand π orbital extended over the whole ligand, with largest value along the C1–C8 bond.

In the complex **2**, the d ruthenium orbitals participate in the molecular orbitals: HOMO−2, HOMO−1, HOMO and LUMO+1, LUMO+2. The bonding MO's are composed from d_{Ru} and π_{Cl}^* orbitals with an admixture of $\pi_{benzene}$. The LUMO orbital is localized on the picoline ring and L+1 is an antibonding orbital of d_{Ru}–benzene. In the L+2 MO's except the part of d_{Ru}–C_6H_6 antibonding, the lone pair of picoline nitrogen participates. The other molecular orbitals are localized mainly on the ligands.

3.3. Electronic spectra

The experimental and calculated, in the TDDFT theory, electronic spectra of [(C_6H_6)RuCl(HBO)] and [(C_6H_6)-$RuCl_2(C_5H_4COOH)$] are presented in Figs. 6 and 7. The contours of calculated spectra were broadened by Lorentzian function calculated by formula:

$$I = \frac{I_0}{1 + \left(\frac{\nu - \nu_0}{\gamma}\right)^2}$$

where $\gamma = 1/2$ of spectral width on 1/2 height.

The assignments of the calculated transitions to the experimental bands are based on the criterion of the energy and oscillator strength of the calculated transitions. In the description of the electronic transitions only the main com-

Table 6
Geometrical parameters for [(C_6H_6)RuCl(HBP)] (**1**)

	Exp.	S_0	S_5	S_6	S_7	T_1	T_7	T_8	T_9
r (Å)									
Ru–Cl1	2.414	2.487	2.525	2.487	2.439	2.494	2.461	2.461	2.495
Ru–O2	2.099	2.093	2.088	2.156	2.048	2.131	2.080	2.080	2.184
Ru–N1	2.080	2.122	2.169	2.184	2.107	2.058	2.118	2100	2.117
Ru–C14	2.157	2.234	2.392	2.479	2.340	2.308	2.310	2.265	2.217
Ru–C15	2.182	2.258	2.307	2.432	2.358	2.392	2.294	2.284	2.274
Ru–C16	2.202	2.242	2.392	2.422	2.390	2.542	2.327	2.268	2.281
Ru–C17	2.160	2.253	2.573	2.403	2.417	2.722	2.338	2.285	2.283
Ru–C18	2.162	2.224	2.714	2.430	2.370	2.725	2.283	2.259	2.305
Ru–C19	2.136	2.241	2.616	2.464	2.336	2.430	2.302	2.271	2.266
O2–C9	1.328	1.309	1.311	1.298	1.327	1.311	1.306	1.312	1.291
C9–C8	1.409	1.433	1.436	1.443	1.440	1.434	1.463	1.436	1.445
C8–C1	1.478	1.436	1.444	1.436	1.424	1.439	1.405	1.394	1.412
C1–N1	1.306	1.322	1.318	1.326	1.347	1.325	1.360	1.375	1.357
Bond angles									
N1–Ru–O2	83.4	84.7	83.4	81.2	85.3	85.8	85.4	86.2	85.1
N1–Ru–Cl1	86.6	85.9	90.2	95.4	90.1	90.4	87.0	86.9	85.8
O2–Ru–Cl1	85.4	86.0	93.6	88.7	91.7	101.4	88.3	87.4	84.7
Ru–O2–C9	124.7	127.9	126.3	126.3	129.9	127.4	132.4	129.9	129.3
O2–C9–C8	124.6	125.0	123.5	123.8	123.0	124.2	123.1	124.7	124.8
C9–C8–C1	120.6	120.3	120.5	120.4	120.7	120.8	121.5	121.5	122.0
C8–C1–N1	125.8	129.3	129.1	129.4	129.8	129.8	130.2	130.1	130.7
Ru–N1–C1	126.2	125.0	122.8	123.3	124.1	125.8	124.4	123.8	124.6
Cl–Ru–C14	114.8	127.4	132.5	132.7	124.9	124.6	122.4	129.6	133.8
Cl–Ru–C15	91.8	97.3	99.5	101.3	95.7	98.8	94.5	98.9	102.0
Cl–Ru–C16	95.9	89.4	87.7	88.2	89.4	97.9	91.3	89.5	90.9
Cl–Ru–C17	122.2	109.5	104.9	102.8	109.6	119.8	113.8	108.1	107.1
Cl–Ru–C18	158.2	145.4	135.1	135.3	143.7	149.6	149.4	143.1	140.8
Cl–Ru–C19	154.3	163.7	156.1	158.7	158.7	159.0	158.1	164.4	167.6
Torsion angles									
Ru–O2–C9–C8	30.0	26.3	35.8	34.1	26.4	23.2	12.6	17.3	12.9
Ru–N1–C1–C8	−13.3	−6.0	−6.8	−13.9	−6.1	−4.0	−9.1	−7.1	−9.3
Ru–O2–C9–C10	−154.4	−155.7	−146.9	−148.6	−155.9	−158.3	−168.0	−164.6	−167.9
Ru–N1–C2–C7	10.6	6.3	6.2	14.9	6.6	3.3	6.6	7.0	8.6
Ru–N1–C2–C3	−169.9	−174.3	−173.5	−165.7	−173.3	−175.9	−174.1	−173.9	−172.4
Ru–N1–C1–O1	170.3	174.5	174.1	166.7	173.5	176.2	173.8	173.9	172.4
O1–C1–C8–C13	−10.6	−8.9	−12.5	−8.5	−6.3	−9.1	−4.5	−4.6	−3.9
N1–Ru–O2–Cl	87.1	86.3	89.8	95.6	89.9	89.6	97.1	87.0	86.2
N1–Ru–O2–C14	−97.1	−87.4	−90.4	−83.6	−90.2	−99.6	−92.9	−89.2	−89.7
N1–C1–C8–C9	−13.3	−10.5	−14.4	−11.4	−8.3	−10.5	−4.0	−5.3	−5.1

ponents of the molecular orbital are taken into consideration.

In Table 4, the singlet electron transitions for $[(C_6H_6)RuCl(HBO)]$ (**1**) calculated in TURBOMOLE program were collected. Only the transitions with large oscillator strengths are shown, with the exception of the lowest electronic transitions where all states are presented, because they can play a role in the photophysical processes. In the calculated spectrum, there are several low energy states (S_1–S_4) with very small oscillator strengths, mainly of $d \rightarrow d$ and $\pi_L \rightarrow d$ origin (LF and LMCT, respectively). They can be compared to the tail in the experimental spectrum near 500 nm. The calculated transition at 392 nm with a large oscillator strength is assigned to the experimental band at 372 nm. This transition is of $\pi_L \rightarrow \pi_L^*$, IL character. Transitions S_6–S_9 with medium oscillator strengths are again of $d \rightarrow d$ and $\pi_L \rightarrow d$ type. The calculated transitions at 326, 288, 285, 281 and 278 are ascribed to the band at 292 nm in the experimental spectrum. The first two of them are of $d \rightarrow \pi_L^*$ (MLCT) character, the remaining ones are LMCT and LL transitions. The transitions calculated below 250 nm are mainly of $\pi_L \rightarrow \pi_L^*$ and $Cl \rightarrow d$ type, and they are attributed to the experimental bands at 248 and 230 nm. One may notice that for Ru(L)(Ben)Cl, the IL state is found at a lower energy than the MLCT state.

In Table 5, 10 calculated triplet states for complex **1** are gathered. The lowest triplet state is found at 666 nm and it has a $\pi_L \rightarrow d$ (LMCT) character. The states T_2–T_5 are of $d \rightarrow d$ (LF) or LMCT type. The state T_6 at 485 nm is of intraligand type (HOMO → LUMO+1). T_8 is of mixed IL/MLCT type, T_9 and T_{10} have LF/LMCT character.

The longest wavelength experimental unsymmetrical band with maximum at 420.4 nm in the complex **2** can be attributed to $d \rightarrow d$ transitions. However, due to some par-

Table 7
The excitation energy of optimized singlet and triplet states for $[(C_6H_6)RuCl(HBP)]$ (**1**)

	Excitation energy ($E_x - E_{SX}$)		Weight	Character	Excitation energy ($E_x - E_{S0}$)	
	E (eV)	λ (nm)			E (eV)	λ (nm)
Singlet states						
S_1	0.19	6588.4	88	$106(d,\pi_L) \rightarrow 107(d,\pi_{Ben}^*)$	1.56	795.2
S_2	1.56	792.6	42	$106(d,\pi_L) \rightarrow 108(d,\pi_{Ben}^*)$	2.08	594.9
			35	$106(d,\pi_L) \rightarrow 107(d,\pi_{Ben}^*)$		
S_3	1.63	762.3	48	$105(d,p_{Cl}) \rightarrow 107(d,\pi_{Ben}^*)$	2.17	570.7
			29	$106(d,\pi_L) \rightarrow 108(d,\pi_{Ben}^*)$		
S_4	1.93	643.4	52	$105(d,p_{Cl}) \rightarrow 107(d,\pi_{Ben}^*)$	2.36	526.3
			17	$106(\pi_L) \rightarrow 108(d,\pi_{Ben}^*)$		
			14	$104(d,p_{Cl}) \rightarrow 108(d,\pi_{Ben}^*)$		
S_5	1.94	637.6	37	$104(d,p_{Cl}) \rightarrow 107(d,\pi_{Ben}^*)$	2.66	466.8
			35	$106(\pi_L) \rightarrow 108(d,\pi_{Ben}^*)$		
			17	$105(d,p_{Cl}) \rightarrow 107(d,\pi_{Ben}^*)$		
S_6	2.28	542.8	44	$104(d,p_{Cl}) \rightarrow 107(d,\pi_{Ben}^*)$	2.80	442.7
			32	$105(d,p_{Cl}) \rightarrow 108(d,\pi_{Ben}^*)$		
S_7	2.83	438.8	47	$106(\pi_L) \rightarrow 108(\pi_L^*)$	3.08	402.9
			13	$104(d,p_{Cl}) \rightarrow 109(d,\pi_{Ben}^*)$		
Triplet states						
T_1	0.39	3191.9	70	$106(d,\pi_L) \rightarrow 107(d,\pi_{Ben}^*)$	1.09	1141.1
			14	$105(d,p_{Cl}) \rightarrow 107(d,\pi_{Ben}^*)$		
T_2	0.72	1710.9	41	$106(\pi_L) \rightarrow 107(d,\pi_{Ben}^*)$	1.45	853.1
			22	$103(d,\pi_L) \rightarrow 107(d,\pi_{Ben}^*)$		
			16	$105(d,p_{Cl}) \rightarrow 107(d,\pi_{Ben}^*)$		
T_3	0.61	2025.1	60	$104(d) \rightarrow 107(d,\pi_{Ben}^*)$	1.57	788.7
			19	$105(d,p_{Cl}) \rightarrow 107(d,\pi_{Ben}^*)$		
T_4	0.91	1357.9	70	$104\ (d,p_{Cl}) \rightarrow 107(d,\pi_{Ben}^*)$	1.67	742.2
			12	$106(\pi_L,d) \rightarrow 108(d,\pi_{Ben}^*)$		
T_5	1.16	1071.8	31	$104(d,p_{Cl}) \rightarrow 107(d,\pi_{Ben}^*)$	1.83	677.4
			24	$105(d,p_{Cl}) \rightarrow 108(d,\pi_{Ben}^*)$		
			14	$105(d,p_{Cl}) \rightarrow 107(d,\pi_{Ben}^*)$		
T_6	1.33	930.5	37	$104(d,p_{Cl}) \rightarrow 108(d,\pi_{Ben}^*)$	1.93	643.5
			14	$105(d,p_{Cl}) \rightarrow 108(d,\pi_{Ben}^*)$		
			14	$105(d,p_{Cl}) \rightarrow 107(d,\pi_{Ben}^*)$		
T_7	2.19	566.8	72	$106(\pi_L) \rightarrow 107(\pi_L^*)$	2.36	525.1
T_8	2.51	493.7	46	$105(d,p_{Cl}) \rightarrow 107(\pi_L^*)$	2.82	440.3
			18	$104(d,p_{Cl}) \rightarrow 107(\pi_L^*)$		
			17	$103(d,\pi_L) \rightarrow 107(\pi_L^*)$		
T_9	2.75	450.9	30	$105(d,p_{Cl}) \rightarrow 108(\pi_L^*)$	2.99	415.0
			23	$104(d,\pi_L) \rightarrow 108(\pi_L^*)$		
			16	$106(\pi_L) \rightarrow 107(d,\pi_{Ben}^*)$		

ticipation of π_{Cl}^* orbitals in the LUMO+1 orbitals, the character of the transitions is described as $d \rightarrow d/\pi^*(Cl)$; in this manner some admixture of the MLCT transition plays a role in the band. The *Metal–Ligand Charge Transfer* ($d \rightarrow \pi_{ligand}^*$) makes the largest contribution into the experimental band at 295.8 nm in the studied complex **2**. The absorption bands at higher energy (272.2, 220.10, 202.6 nm for complex **2**) are assigned to *Ligand–Metal Charge Transfer* ($\pi_{ligand} \rightarrow d$) and intra- and inter *Ligand–Ligand Charge Transfer* transitions (see Fig. 8).

3.4. Emission property of the $[(C_6H_6)RuCl(HBO)]$ and luminescence mechanism

An emission property of the studied complex **1** has been examined in the acetonitrile solution at room temperature. The luminescence spectra are presented in Fig. 9. The complex **1** was excited at 375 nm, the emission peaks were observed at 518 and 551 nm with the shoulder with maximum at 457 nm.

We attempted to optimize the geometry for several low lying singlet and triplet excited states of $[(C_6H_6)RuCl(HBO)]$. Energy of the first singlet excited state during optimization gets very close to the ground state energy, and then starts to oscillate. Next three states are close in energy and the optimization could not be completed, too. All these states are of LF and LMCT character. The optimization of states S_5–S_7 was successful. The optimized geometry of the ground state and the experimental geometry of $[(C_6H_6)RuCl(HBO)]$ is given in Table 6. The energies of the optimized excited states are gathered in Table 7 and the orbital excitations with largest weights are shown in Fig. 10.

The geometry of the ground state from optimization with the COSMO solvent model is presented in Table 3. The PCM optimization gives very close parameters, the differences are in range of 0.01 Å for bond lengths and 2° for bond angles. The calculated ground state geometry agrees well with the crystal structure; the largest differences are for Ru–Cl bond (~0.06 Å) and the average length of the $Ru–C_{ben}$ bond (~0.07 Å).

In the excited states S_5–S_7, the most pronounced geometry changes are related to the $Ru–C_{ben}$ distances. In S_5 state, the Ru–C distances of three benzene carbons are much longer than those of the three remaining ones, which means that the benzene ring is shifted and tilted. In S_6 and S_7 states, the $Ru–C_{ben}$ distances do not differ very much, but in S6 they are longer than in S_7. S_5 and S_6 are LF states, as it can be seen in Fig. 6. The unoccupied d orbitals are mixed in antibonding manner with benzene π orbitals, which results in loosening the benzene ligand bonding. S7 has mainly intraligand $\pi_L \rightarrow \pi_L^*$ character. It corresponds to the sixth excited state in the vertical spectrum, which implies that another excited state gets lower energy in the

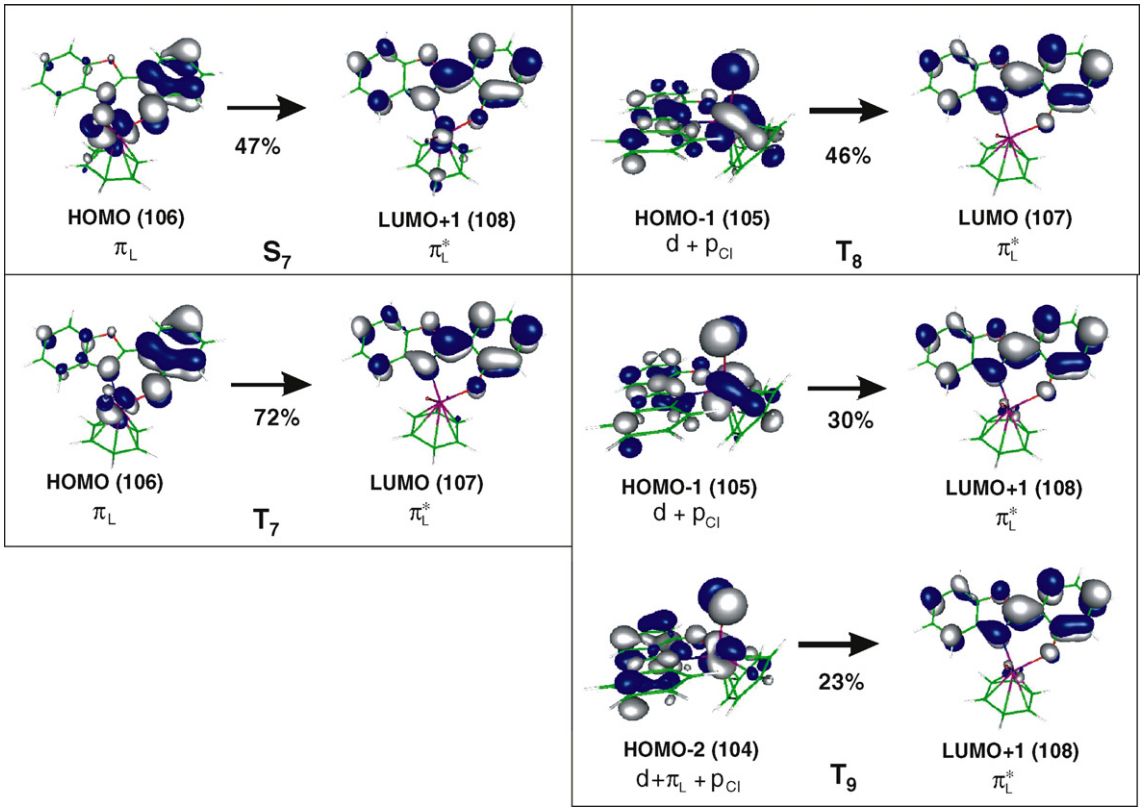

Fig. 10. Character of excited states participating in luminescence according to TDDFT calculations in $[RuCl(CO)(PPh_3)_2(C_9H_6NO)]$.

course of the optimization. Comparing the HOMO orbital from Fig. 6 with relevant orbital from Fig. 1, one can see that this orbital has a larger contribution from metal d orbital, and in its minimum the S_7 state acquires some MLCT character. This state has also some LF content (about 13%) which explains the longer bonds with benzene carbons. The excitation energy for this state in its equilibrium geometry is 2.83 eV which corresponds to 438 nm (Table 4).

The optimization was also carried out for several triplet states. The difference between the triplet excited state and ground state energy in the excited state minimum geometry for the effectively optimized states is given in Table 4 and their geometry is gathered in Table 3. In Fig. 2, the orbital excitations for these states are depicted. The first triplet state T_1 was optimized by independent DFT calculations. The minimum of this state is very close to the ground state ($\Delta E = 0.11$ eV). This state has a LF character. In this state, the benzene ring is also shifted and tilted, as can be seen in Table 3. The energy of T_2–T_6 goes down significantly during optimization, but because of a near degeneracy their optimization could not be finished. These states are of LF or LMCT character. We were able to optimize states T_7, T_8 and T_9. T_7 is basically a IL state, T_8 and T_9 are of MLCT type. The geometry parameters for these states are gathered in Table 6 and the most important excitations are depicted in Fig. 10. It can be seen from Table 6 that ruthenium–benzene carbon bonds are elongated in T_7, T_8 and T_9 but to a smaller extent than in T_1, S_5 and S_6. The C8–C1 bond is shorter in T_7–T_9 and the torsion angle N1–C1–C8–C9 is smaller, which indicates that the ligand is more rigid in these states. The excitation energies for these states are 565, 493 and 450 nm, respectively.

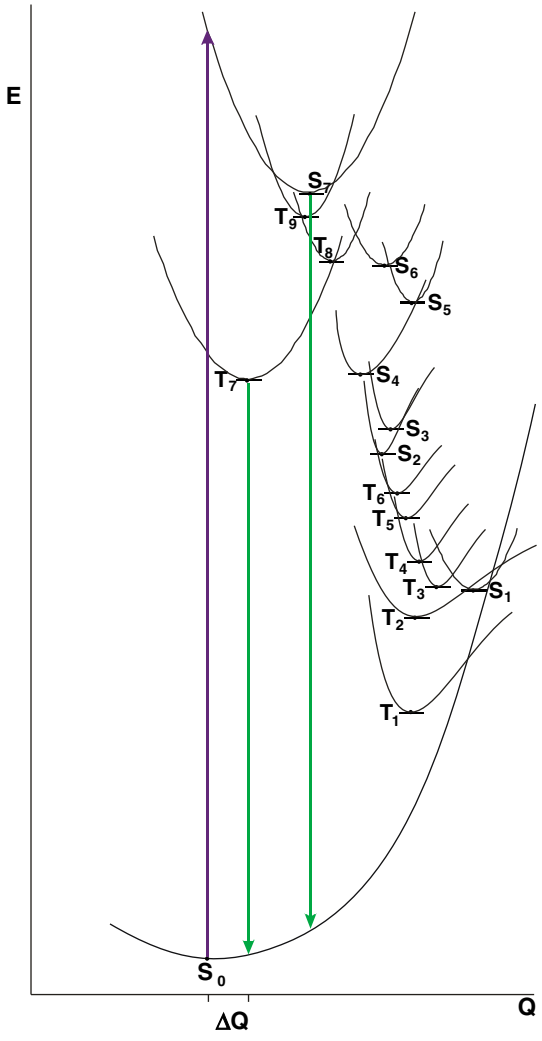

Fig. 11. Schematic representation of the ground state and excited states of Ru(L)(Ben). Purple arrow denotes absorption, green arrow – luminescence. (For interpretation of the references to colour in this figure legend, the reader is referred to the Web version of this article.)

In Fig. 11, the schematic representation of the ground state and excited states of [(C_6H_6)RuCl(HBO)] is given. On the basis of TDDFT calculations, we may propose the luminescence mechanism of [(C_6H_6)RuCl(HBO)]. The excitation to the intense band at 372 nm (calculated at 392 nm) of primarily LF character and geometry relaxation (state S_7) the molecule through intersystem crossing goes to T_9 and next through internal conversions to T_8 and T_7. All these states can be luminescent; their calculated energies agree well with experimental luminescence wavelengths, 456, 518 and 551 nm. The complicated structure of the luminescence spectrum suggests that more than one state is involved in luminescence process. Hence the luminescence is of IL/MLCT origin in this system. The location of these states relatively to the ground state minimum shows that they are characterized by a relatively small geometry distortion. The singlet and triplet states of LF and LMCT type, which are close to the ground state energy surface, can provide the radiationless deactivation channel for [(C_6H_6)RuCl(HBO)].

4. Conclusion

The two new half-sandwich complexes of ruthenium with N-heterocyclic ligands (2-(2′-hydroxyphenyl)-benzoxazole and 4-picolinic acid) have been prepared and studied by IR, UV–Vis spectroscopy and X-ray crystallography. The molecular orbital diagrams of the complexes has been calculated with the density functional theory (DFT) method. The electronic spectra of the obtained compounds have been calculated using the TDDFT method. The luminescence property of the one of the half sandwich complex – [(C_6H_6)RuCl(HPB)] – was studied by the DFT method and the mechanism was suggested.

5. Supplementary material

CCDC 645465 and 646157 contains the supplementary crystallographic data for **1** and **2**. These data can be obtained free of charge from The Cambridge Crystallographic Data Centre via www.ccdc.cam.ac.uk/data_request/cif.

Acknowledgement

Crystallographic part was financed by funds allocated by the Ministry of Scientific Research and Information Technology to the Institute of General and Ecological Chemistry, Technical University of Łódź. The GAUSSIAN03 calculations were carried out in the Wrocław Centre for Networking and Supercomputing, WCSS, Wrocław, Poland under calculational Grant No. 51/96.

References

[1] M. Navarro, W.F.D. Giovani, J.R. Romero, Synth. Commun. 20 (1990) 399.
[2] N. Grover, H.H. Thorp, J. Am. Chem. Soc. 113 (1991) 7030.
[3] X. Hua, M. Shang, A.G. Lappin, Inorg. Chem. 36 (1997) 3735.
[4] C.M. Che, C. Ho, T.C. Lau, J. Chem. Soc., Dalton Trans. (1991) 901.
[5] S.J. Raven, T.J. Meyer, Inorg. Chem. 27 (1988) 4478.
[6] C.M. Che, W.T. Tang, W.O. Lee, K.Y. Wong, T.C. Lau, J. Chem. Soc., Dalton Trans. (1992) 1551.
[7] A. Dovletoglou, S.A. Adeyemi, M.N. Lynn, D.J. Hodgson, T.J. Meyer, J. Am. Chem. Soc. 112 (1990) 8989.
[8] C.M. Che, V.W.W. Yam, Adv. Inorg. Chem. 39 (1992) 233.
[9] R.A. Binstead, M.E. McGuire, A. Dovletoglou, W.K. Senk, L.E. Roecker, T.J. Meyer, J. Am. Chem. Soc. 114 (1992) 173.
[10] J.W. Faller, A. Lavoie, J. Organomet. Chem. 630 (2001) 17.
[11] D.L. Davies, J. Fawcett, S.A. Garrat, D.R. Russel, Organometallics 20 (2001) 3029.
[12] L.F. Szszepura, S.M. Maricich, R.F. See, M. Rowen Churchill, K.J. Takeuchi, Inorg. Chem. 34 (1995) 4198.
[13] S. Bennett, S.M. Brown, G. Conole, M. Kessler, S. Rowling, E. Sinn, S. Woodward, J. Chem. Soc., Dalton Trans. 3 (1995) 367.
[14] Y. Miyaki, T. Onishi, H. Kurosawa, Inorg. Chim. Acta 300/302 (2000) 369.
[15] H. Asano, K. Katayama, H. Kurosawa, Inorg. Chem. 35 (1996) 5760.
[16] B.M. Holligan, J.C. Jeffery, K. Norgett, E. Schatz, M.D. Ward, J. Chem. Soc., Dalton Trans. (1992) 3345.
[17] J.T. Groves, M. Bonchio, T. Carofiglio, K. Shalyaev, J. Am. Chem. Soc. 118 (1996) 8961.
[18] W.P. Griffith, Trans. Met. Chem. 15 (1990) 251.
[19] T.C. Lau, C.M. Che, W.O. Lee, C.K. Poon, J. Chem Soc., Chem. Commun. (1988) 1406.
[20] M. Bressan, A. Morvillo, J. Chem. Soc., Chem. Commun. (1989) 421.
[21] A. Fernandez-Ramosa, J. Rodrıguez-Otero, M.A. Rıos, J. Soto, J. Mol. Struct. (Theochem) 489 (1999) 255.
[22] W. Sanger, Principles of Nucleic Acid Structure, Springer-Verlag, NewYork, 1984.
[23] D.L. Williams, A. Heller, J. Phys. Chem. 74 (1970) 4473.
[24] J. Catal'an, F. Fabero, M.S. Guijarro, R.M. Claramunt, M.D.S. Maria, M.C. Foces-Foces, F.H. Cano, J. Elguero, R. Sastre, J. Am. Chem. Soc. 112 (1990) 747.
[25] L.M. Tolbert, K.M. Solntsev, Acc. Chem. Res. 35 (2002) 19.
[26] Rodrigo S. Iglesias, Paulo F.B. Goncalves, Paolo R. Livotto, Chem. Phys. Lett. 327 (2000) 23.
[27] Y. Zhang, X.-D. Yang, K. Wang, D.C. Crans, J. BioInorg. Chem. 100 (2006) 80;
S. Chaudhary, J. Pinkston, M.M. Rabile, J.D. Van Horn, J. BioInorg. Chem. 99 (2005) 787;
D.D.D. Hepburn, J.B. Vincent, J. BioInorg. Chem. 94 (2003) 86.
[28] S. Park, Y. Do, J. Organomet. Chem. 692 (2007) 1633.
[29] GAUSSIAN03, Revision B.03: M.J. Frisch, G.W. Trucks, H.B. Schlegel, G.E. Scuseria, M.A. Robb, J.R. Cheeseman, J.A. Montgomery, Jr., T. Vreven, K.N. Kudin, J.C. Burant, J.M. Millam, S.S. Iyengar, J. Tomasi, V. Barone, B. Mennucci, M. Cossi, G. Scalmani, N. Rega, G.A. Petersson, H. Nakatsuji, M. Hada, M. Ehara, K. Toyota, R. Fukuda, J. Hasegawa, M. Ishida, T. Nakajima, Y. Honda, O. Kitao, H. Nakai, M. Klene, X. Li, J.E. Knox, H.P. Hratchian, J.B. Cross, C. Adamo, J. Jaramillo, R. Gomperts, R.E. Stratmann, O. Yazyev, A.J. Austin, R. Cammi, C. Pomelli, J.W. Ochterski, P.Y. Ayala, K. Morokuma, G.A. Voth, P. Salvador, J.J. Dannenberg, V.G. Zakrzewski, S. Dapprich, A.D. Daniels, M.C. Strain, O. Farkas, D.K. Malick, A.D. Rabuck, K. Raghavachari, J.B. Foresman, J.V. Ortiz, Q. Cui, A.G. Baboul, S. Clifford, J. Cioslowski, B.B. Stefanov, G. Liu, A. Liashenko, P. Piskorz, I. Komaromi, R.L. Martin, D.J. Fox, T. Keith, M.A. Al-Laham, C.Y. Peng, A. Nanayakkara, M. Challacombe, P.M.W. Gill, B. Johnson, W. Chen, M.W. Wong, C. Gonzalez, J.A. Pople, Gaussian Inc., Pittsburgh, PA, 2003.
[30] A.D. Becke, J. Chem. Phys. 98 (1993) 5648.
[31] C. Lee, W. Yang, R.G. Parr, Phys. Rev. B 37 (1988) 785.
[32] M.E. Casida, in: J.M. Seminario (Ed.), Recent Developments and Applications of Modern Density Functional Theory, Theoretical and Computational Chemistry, vol. 4, Elsevier, Amsterdam, 1996, p. 391.
[33] K. Eichkorn, F. Weigend, O. Treutler, R. Ahlrichs, Theor. Chim. Acc. 97 (1997) 119.
[34] G.M. Sheldrick, Acta Crystallogr. A46 (1990) 467.
[35] G.M. Sheldrick, SHELXL97. Program for the Solution and Refinement of Crystal Structures. University of Göttingen, Germany, 1997.
[36] G.M. Sheldrick, SHELXTL: Release 4.1 for Siemens Crystallographic Research Systems, 1990.
[37] A. Singh, N. Singh, D.S. Pandey, J. Organomet. Chem. 642 (2002) 48.
[38] U. Beck, W. Hummel, H.B. Burgi, A. Ludi, Organometallics 6 (1993) 20.
[39] F.B. McCormick, D.D. Cox, W.B. Gleason, Organometallics 12 (1993) 610.
[40] J.G. Małecki, J.O. Dzięgielewski, M. Jaworska, R. Kruszynski, T.J. Bartczak, Polyhedron 23 (2004) 885.
[41] R. Tribo, J. Pons, R. Yanez, J.F. Piniella, A. Alvarez-Larena, J. Ros, Inorg. Chem. Commun. 3 (2000) 545;
M. Jahncke, A. Neels, H. Stoeckli-Evans, G. Süss-Fink, J. Organomet. Chem. 561 (1998) 227;
H. Kurosawa, H. Asano, Y. Miyaki, Inorg. Chim. Acta 270 (1998) 87.
[42] G.R. Desiraju, T. Steiner, The Weak Hydrogen Bond in Structural Chemistry and Biology, Oxford University Press, 1999.
[43] G.A. Jeffrey, W. Saenger, Hydrogen Bonding in Biological Structures, Springer-Verlag, 1994.
[44] R. Taylor, O. Kennard, J. Am. Chem. Soc. 104 (1982) 5063.